Common-mode rejection in the measurement of wearable ECG with cooperative sensors

Methods

Michaël Rapin*, Yves-Julien Regamey and Olivier Chételat

Common-mode rejection in the measurement of wearable ECG with cooperative sensors

Gleichtaktunterdrückung von EKG-Messungen mittels tragbaren kooperativen Sensoren

Toward a new generation of medical-quality ECG Holter with dry electrodes

Eine neue Generation von medizinischen EKG-Holter mit Trockenelektroden

https://doi.org/10.1515/auto-2018-0061
Received May 1, 2018; accepted October 4, 2018

Abstract: Recently, telemonitoring of vital signs has gained a lot of research interest. Especially for electrocardiogram (ECG), which is among the most frequently measured vital sign. However, the integration of classical ECG Holter in wearables is problematic since shielded cables and gel electrodes are required to get ECG signals of highest quality. We have recently introduced a novel sensing architecture based on active electrodes (so-called cooperative sensors) that significantly reduces the cabling complexity of the monitoring device. After briefly recalling the principle of cooperative sensors this paper details how they address rejection of common-mode voltage induced by electromagnetic disturbances. The proposed approach uses an auto-identification technique based on a continuous-time calibration of the sensor system and a digital control loop. To demonstrate the reliability of the proposed approach, a 12-lead ECG monitoring system was implemented with the new common-mode rejection method. Measurements on four healthy volunteers showed that the signal quality obtained with the cooperative-sensor system (using dry electrodes) is equivalent to the one measured with a gold standard medical device (using gel electrodes) in exercise stress tests.

Keywords: wearable sensors, electrocardiography (ECG), common-mode rejection, active electrodes, dry electrodes, cooperative sensors, telemonitoring

***Corresponding author: Michaël Rapin,** Laboratory for Orthopedic Biomechanics, Swiss Federal Institute of Technology in Zurich (ETHZ), Zürich 8092, Switzerland; and Centre Suisse d'Electronique et de Microtechnique (CSEM), Neuchatel 2002, Switzerland, e-mail: mir@csem.ch
Yves-Julien Regamey, Olivier Chételat, Centre Suisse d'Electronique et de Microtechnique SA, Rue Jaquet-Droz 1, CH-2002 Neuchatel, Switzerland, e-mail: och@csem.ch

Zusammenfassung: In jüngster Zeit wurde dem Telemonitoring von Vitalfunktionen viel Forschungsinteresse gewidmet. Insbesondere dem Elektrokardiogramm (EKG), welches zu den am häufigsten gemessenen Vitalparametern gehört. Die Integration von klassischen EKG-Holter in tragbaren Geräten ist problematisch, da es Gel-Elektroden und geschirmte Kabel erfordert, um hochqualitative EKG-Signale messen zu können. Wir haben kürzlich eine neuartige Sensorik-Architektur eingeführt, welche auf aktiven Elektroden basiert (sogenannte kooperative Sensoren) und die Verkabelungskomplexität erheblich reduziert. In der vorliegenden Arbeit beschreiben wir zuerst kurz das Funktionsprinzip der kooperativen Sensoren, gefolgt vom neuartigen Ansatz zur Gleichtaktunterdrückung. Der vorgeschlagene Ansatz verwendet eine automatische Identifikationstechnik, basierend auf einer zeitkontinuierlichen Kalibrierung des Sensorsystems mittels einem digitalen Regelkreis. Um dessen Zuverlässigkeit zu testen, wurde das vorgeschlagene Verfahren zur Gleichtaktunterdrückung in einem 12-Kanal EKG-System implementiert. Messungen an vier gesunden Probanden haben gezeigt, dass die kooperativen Sensoren (mit Trockenelektroden) im Vergleich zum medizinischen Goldstandard (mit Gel-Elektroden) gleichwertige Signalqualität während Belastungstests liefern.

Schlagwörter: Tragbare Sensoren, Elektrokardiographie (EKG), Gleichtaktunterdrückung, aktive Elektroden, Trockenelektroden, kooperative Sensoren, Telemonitoring

1 Introduction

Telemonitoring of vital signs can enable novel clinical strategies [1, 2]. Patients suffering from chronic diseases, such as congestive heart failure (CHF), could benefit from

remote, continuous monitoring [3]. An essential requirement for telemonitoring systems is ease of use [4]. At the same time, telemonitoring systems need to be highly integrated so that patients can monitor their vital signs during their daily-life with minimal inconvenience. Moreover, the development of miniaturized sensing technologies, together with the spread of consumer electronics (smartphones, tablets, etc.) and a growing attention from individuals have further driven the transition from bedside monitoring systems towards wearable devices, allowing people to access their physiological state anytime in their daily life [5].

Electrocardiogram (ECG) is among the most frequently measured vital signs. Classical approaches to measure high-quality ECG require the use of shielded or multi-wire cables which are connected to a central unit in a star arrangement [6, 7]. Consequently, with the classical approach, any additional lead directly increases the cabling complexity to the central unit and the size of the device might be limited by the size of the cables and connectors. Many wearable ECG monitoring devices—also called ECG Holter—have been developed and placed on the market. However, their integration in wearables is problematic since they require shielded cables and gel electrodes to get high-quality ECG signals.

An alternative to the star arrangement is to connect active sensors in a chain (or bus) configuration [8]. This way, the number of wires connected to each active sensor does not increase when the number of leads increases. However, multi-wire cables with complex insulation, shielding, and connectors are still required [9], creating a bottleneck towards smaller and cheaper wearables.

We recently proposed a novel electrical architecture based on dry-electrode active sensors (so-called cooperative sensors) which significantly reduces the cabling complexity of the sensor system [10]. In brief, only two unshielded wires link all cooperative sensors in a bus arrangement. Consequently, the number of sensors does not limit the sensors miniaturization. The first wire provides the common reference voltage necessary for biopotential measurements and is used together with the second wire for synchronization and communication between the cooperative sensors. This approach allows eliminating shielded or complex multi-wire cables. The common mode induced by electromagnetic disturbances on the unshielded wires is attenuated via a basic digital feedback loop [11].

In this paper, section 1 presents the basics of ECG measurement and briefly recalls why classical approaches used to measure ECG use a central electronic unit and shielded cables. Then, section 2 introduces the cooperative sensor and details the basic common-mode rejection approach used by this new electrical architecture. Section 2 also gives more details about the functional diagram of cooperative sensors and shows how it is possible to improve the global common-mode rejection ratio (CMRR) of the cooperative-sensor system with a continuous-time system calibration, which is the main innovation presented in this paper. Finally, section 3 shows the implementation of the cooperative-sensor system in a wearable 12-lead ECG monitoring system demonstrating the reliability of the proposed approach for wearable dry-electrode high-quality ECG monitoring in real-life scenario. Section 4 concludes this paper.

1.1 Classical circuit for multilead ECG measurement

Fig. 1 shows the classical approach for ECG measurement. Basically, the ECG signal is modeled as a voltage source u_{ECG} located in the body, while skin impedances z_g, z_1, and z_2 model the impedances of the electrode-body interfaces. The ECG voltage u_{ECG} is obtained by measuring the voltage difference u_2-u_1. In practice, electromagnetic disturbance can be modeled by a current source injecting a current into the exposed conductor (see i_{em} in Fig. 1). When the current i_{em} is injected at any point of the exposed lines, a part of it may cross the skin impedances. As these impedances are

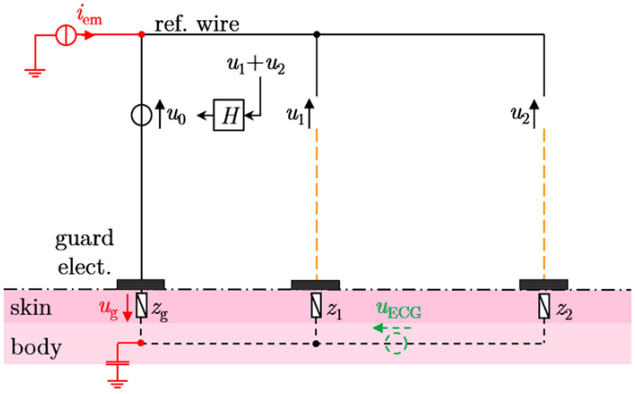

Figure 1: Classical circuit for ECG measurement with a common-mode voltage controller. Here, u_{ECG} represents the ECG voltage, u_1 and u_2 the measured voltages, u_g the disturbance voltage resulting from the current i_{em} (induced by electric-field variations) flowing toward the earth ground via the skin impedance z_g. The controller H controls the common-mode voltage to zero via the voltage source u_0 in order to compensate u_g. The ECG voltage u_{ECG} is obtained by measuring the voltage difference u_2-u_1. The impedances z_g, z_1, and z_2 are the skin impedances beneath the guard electrode and the branches used to measure u_1 and u_2.

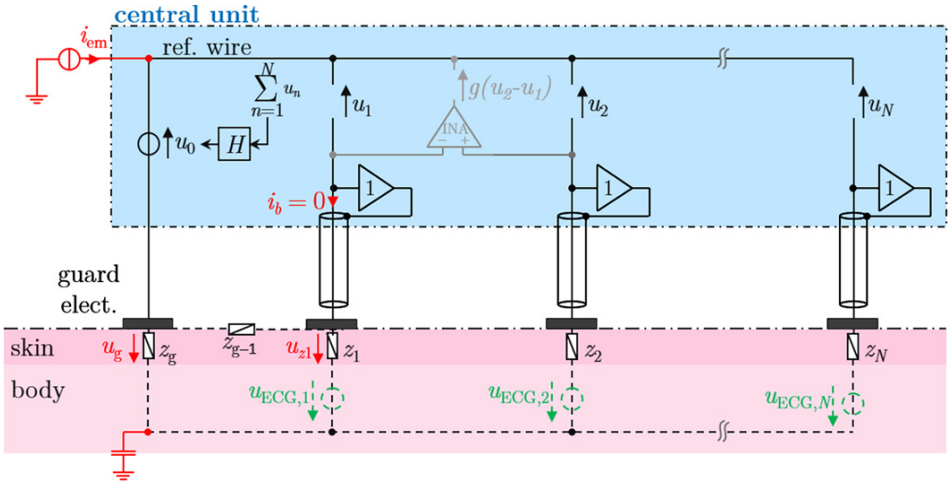

Figure 2: Classical circuit for multilead ECG measurement with a central unit and shielded cables. The ECG leads are obtained via linear combinations of the voltages measured as u_1 to u_N.

relatively large, this leads to a significant voltage u_g in series with the ECG voltage which directly affects the ECG signals measured at u_1 and u_2. Since the disturbance voltage u_g is identically measured by both u_1 and u_2, it is cancelled by doing the difference between u_1 and u_2.

The disturbance voltage u_g however affects the amplifier common-mode voltage which is defined as $(u_1 + u_2)/2$. Depending on the CMRR of the amplifier circuits used to measure u_1 and u_2, the differences (i. e., the measured ECG signal) may still be affected by the common-mode voltage. Moreover, the common mode may also induce a saturation of the circuits used to amplify the measured voltages. The classical approach used to solve this issue is to control the common mode to zero via the controller H and the controlled voltage source u_0 (see Fig. 1).

A closer look on the circuit presented in Fig. 1 shows that any current injected in the section that is marked in dashed orange still generates a voltage disturbance on u_1 and/or u_2, and therefore affect the measured ECG. To further reduce the sensitivity to noise of this circuit, shielded cables are used, leading to the classical circuit for ECG measurement shown in Fig. 2. Besides the guard electrode and the common-mode controller H, shielded cables are used to connect the passive electrodes to the central unit which contains all electronic circuits required for the measurement. These shields are driven with the same potentials as the ones measured on the cable cores to guarantee high input impedances, which is essential to ensure a high-quality ECG signal [12, 13] (see also section 1.3). It has to be noted that additional ECG leads can be obtained by simply adding replicates of the branch used to measure u_1 or u_2. The ECG leads are then obtained via the difference (or a linear combination) between the voltages measured by the different branches. A classical approach to measure this difference is to use an instrumentation amplifier (INA) as shown in Fig. 2. The next three subsections detail three sources of error commonly known to affect the ECG measurement with the classical circuit shown in Fig. 2.

1.2 Analog frontend bias current

In practice, a low bias current of the analog frontend used to sense u_1 to u_N is required to guarantee a high-quality ECG measurement. Indeed, as a first approximation the voltages on the skin impedances z_1 to z_N (see Fig. 2) are equal to zero since the currents in the voltage-measurement branches are considered as null. However, actual analog frontends have bias currents (i_b) flowing through these skin impedances that may induce a significant voltage on the measured signal. Consequently, any changes in the skin impedance values, for instance due to the motion on the electrode-body interface, may generate motion artifacts on the measured voltages [13]. For this reason, it is important to minimize both the skin impedance and the bias current of the analog frontends. This effect is even more important if dry electrodes are used since they are usually characterized by a higher skin-contact impedance [14].

1.3 Analog frontend input voltage divider

Another issue related to the sensing circuits is the voltage divider embodied by the skin impedance and the input impedance of the voltage-sensing analog frontend [12]

which attenuates the measured ECG signal according to the following equation:

$$u_n = u_{ECG,n}\frac{z_{in,n}}{z_{in,n} + z_n}$$

where u_n and $u_{\mathrm{ECG},n}$ are the voltages measured and seen by the n^{th} measurement branch, respectively (with $n \in \{1, ..., N\}$). The impedance $z_{\mathrm{in},n}$ is the input impedance of the analog frontend of the n^{th} branch, and z_n its corresponding skin impedance. It is thus important to maximize the input impedance of the analog frontends. Here as well, this effect is even more important for high skin-contact impedances (i. e., if dry electrodes are used).

It has to be noted that this signal attenuation may also influence the CMRR. Indeed, since the skin impedances z_1 to z_N vary from one voltage-sensing branch to the other, the amplitude of the residual common-mode voltage measured by the sensors will not be the same for all branches. Consequently, the common mode is incompletely cancelled when the difference between the voltages measured at u_1 to u_N is performed.

1.4 Effect of the surface skin impedance on the disturbance voltage rejection

As a first approximation, we can model the skin impedance under the guard electrode as z_{g} and the skin impedance under the branch used to sense u_1 as z_1, (see Fig. 2). The impedance at the surface of the skin between these two electrodes can be modeled as $z_{\mathrm{g-1}}$. From this model, it is possible to compute the disturbance voltage u_{z1} due to i_{em} flowing through the resistor network—modeled by z_{g}, z_1, and $z_{\mathrm{g-1}}$—toward the earth ground via the guard electrode. The following equation shows that the disturbance voltage u_{z1} increases if the impedance $z_{\mathrm{g-1}}$ decreases, meaning that a low impedance between the electrodes results in a disturbance voltage measured as u_1, consequently, the guard electrode must be placed away from the voltage-sensing electrodes (used to measure u_1 to u_N). A similar equation is also applicable for the disturbance voltages measured by the other sensors (i. e., u_{z2} to u_{zN}).

$$u_{z1} = z_1\frac{z_g}{z_g + z_{g-1} + z_1}i_{em}$$

2 Common-mode rejection with cooperative sensors

While the previous section shows the classical approach used to measure ECG of high quality, this section recalls the concept of cooperative sensors and shows a method to improve the CMRR with this new architecture.

2.1 The cooperative sensor principle

The cooperative-sensor architecture keeps the same underlying electrical architecture (see Fig. 2) but the central unit is removed and the electronic circuits are placed directly onto the skin. The length of cables sensitive to electric-field disturbance is thus reduced to its minimum. This architecture is based on active sensors connected in a bus arrangement with two unshielded wires, the reference wire (ref. wire) and the communication wire (com. wire). As shown in Fig. 3, the system is made of one master sensor, one reference sensor, and at least one voltage-sensing (type V) sensor. Each sensor has its own power supply (a battery) and a single contact with the skin implemented as a stainless steel electrode.

The ref. wire sets the common analog reference potential required for ECG measurements. Any sensor-specific potential on the skin is therefore measured with respect to this wire. The voltages u_1 to u_N are amplified, filtered, and digitized locally by the electronic circuit embedded in each sensor.

The communication from the master sensor to the reference and type V sensors is performed via voltage impulses sent by v_0. The signal v_0 is also used by the reference and type V sensors to recover the master clock via a clock-data recovery mechanism. The communication from the reference and type V sensors to the master sensor is performed via current impulses sent by i_1 to i_N and sensed as i_0 in the master sensor. The cooperative sensors are thus connected in a two-wire bus configuration and data acquired by the reference and type V sensors are gathered in the master sensor [10].

2.2 Common-mode rejection principle

In the architecture of Fig. 3, the voltage u_1 is measured in the reference sensor, its digitized value is sent to the master sensor, and controlled to zero via the voltage source u_0. Consequently, the disturbance voltage u_{g} induced by i_{em} flowing through z_g is readily compensated via the common-mode controller which controls u_0. In this configuration, the common mode is not strictly zero since only the voltage u_1 is controlled to zero. However, the effect of the disturbance voltage u_{g} is compensated.

With this configuration, the feedback loop allowing the common-mode rejection includes the digital commu-

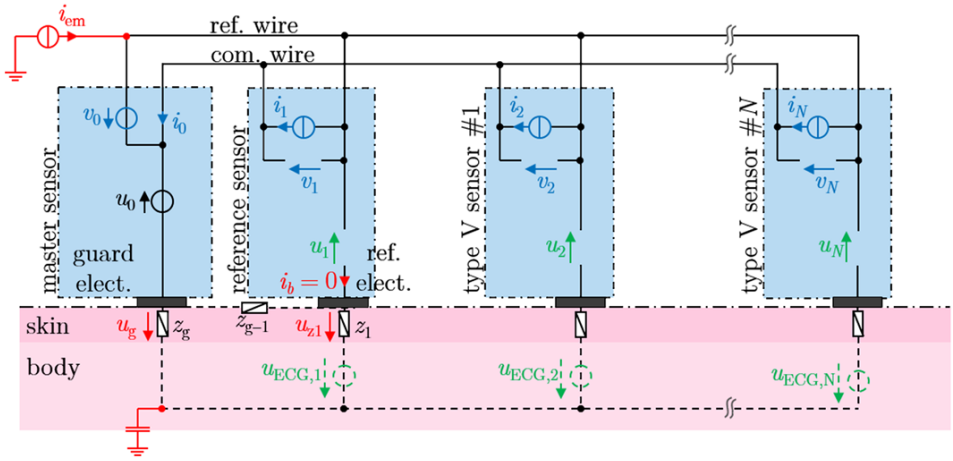

Figure 3: Architecture for common-mode rejection with cooperative sensors. All sensors have one contact with the skin and two electrical contacts with the external wires (ref. and com. wires). The voltage u_1 measured by the reference sensor is sent to the master sensor and controlled to zero via the voltage source u_0.

nication bus, the sampling frequency of u_1 needs to be fast enough to allow a good rejection of the common-mode voltage. The best open-loop transfer function is basically $(z-1)^{-1}$, resulting in the rejection of the disturbance voltage u_g by $||1-z^{-1}||$, or by $||1-e^{-j2\pi f/f_s}||$. Here, z corresponds to the z-transform variable, f_s is the sampling frequency of u_1, and f any frequency to be rejected. As an example, for $f_s = 50$ kHz, one gets a maximal rejection factor of 159 for mains disturbances (i. e., for $f = 50$ Hz), which corresponds to an attenuation of the common mode ($\mathrm{CMRR_{FB}}$) of 44 dB. Even if this attenuation prevents the saturation of the amplifier used to measure u_1 to u_N, the rejection is not ideal and a residual common-mode voltage is present on the measured voltages. This common-mode voltage is further attenuated when computing the final ECG leads which are defined as the differences (or a linear combination) between the measured voltages. In the cooperative sensor architecture, the voltages u_1 to u_N are amplified, filtered, and digitized by different analog chains implemented in each sensors. Consequently, the matching between the transfer functions of each measuring sensor impacts the common-mode rejection. The common-mode attenuation of the differential stage ($\mathrm{CMRR_D}$) is related to the following equation:

$$\mathrm{CMRR_D} = -20\log\left((1+P_G)-(1-P_G)\right) = -20\log\left(2P_G\right)$$

where P_G is the precision of the gain of a cooperative-sensor analog chain at a given frequency. As an illustration, for a gain accuracy of ±1 % ($P_G = 0.01$), the $\mathrm{CMRR_D}$ is equal to 34 dB (in the worst case). This results in a total CMRR of the cooperative-sensor system of 78 dB ($= \mathrm{CMRR_{FB}} + \mathrm{CMRR_D}$).

The problem of mismatch between active sensors has already been mentioned in the literature. To improve the CMRR of their system, Degen and Jäckel [15] use the 50 Hz interference as common-mode signal to adjust the gain of their active electrodes. In our work, section 2.3 shows a method for the auto-identification and the rectification of the transfer functions over the whole bandwidth of the cooperative-sensor system based on a perturbation voltage in the form of a train of pulses added to the intrinsic common-mode potential.

2.3 Auto-identification of transfer functions and rectification

The idea behind this auto-identification is to send a common identification signal to all measuring sensors via the voltage source u_0 embedded in the master sensor. Fig. 4 shows the functional diagram corresponding to the electrical architecture shown in Fig. 3. The common excitation corresponds to the signal d. This functional diagram also includes post filtering transfer functions H_1 to H_N. The transfer function G_0 is a constant, G_1 an integrator implemented in the reference sensor, and G_2 to G_N the band-pass filters of the type V sensors.

The main goal of post processing is to correct the implemented transfer functions of the acquisition chains to get exactly the transfer function between $u_{\mathrm{ECG},n}$ and U_n (with $n \in \{1,\ldots,N\}$) defined by international standard IEC 60601-2-25, i. e., a high-pass filter at 0.05 Hz and a low-pass filter at 150 Hz, both first order. Having exactly this transfer function for all measured biopotential (u_1 to u_N) implies

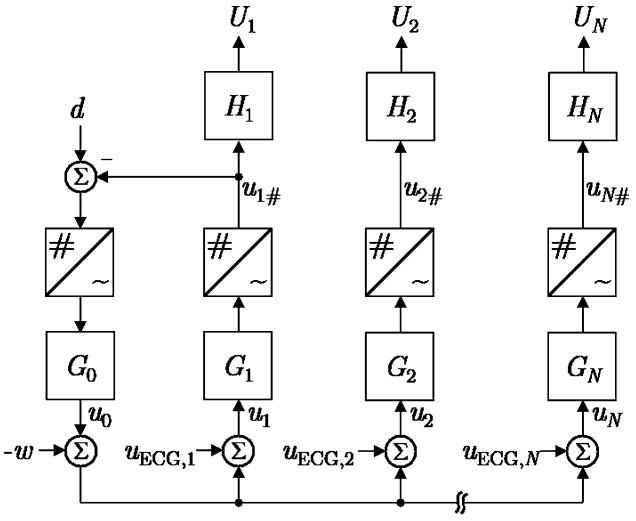

Figure 4: Functional diagram of the biopotential measurement chains including the master sensor (index number 0), the reference sensor (index number 1), and type V sensors number 2 and *N*. The common excitation corresponds to the signal *d*. The implemented transfer functions G_n are corrected by the transfer functions H_n. The noise is represented as a voltage signal by *w*.

that any difference between two measured biopotentials is not affected by the common mode.

The principle to get exact transfer functions is to identify the implemented transfer functions G_n and to correct them by the transfer functions H_n which are the combination of the inverse of G_n and the targeted transfer function. The identification can be performed online with signal d as known excitation. The transfer function between d (the excitation signal) to $u_{n\#}$ (the signal at the output of each ADC) is:

$$\frac{u_{n\#}}{d} = \frac{[G_n G_0]}{1 + [G_n G_0]}$$

where the brackets are used to modify a continuous transfer function $G_n(s)$ to its discrete equivalent when ADC and DAC are used:

$$[G] = \left(1 - z^{-1}\right) ZL^{-1} \frac{G}{s}$$

with L^{-1} the inverse Laplace transform and Z the z-transform. As G_0 is a constant transfer function, the common-mode signal u_0 generated by d is filtered by a high-pass filter. This filter is correctly described by:

$$\frac{G_0}{1 + [G_1 G_0]}$$

which can be approximated for low frequencies by:

$$\frac{1}{G_1} = s\tau$$

Therefore, if d is a square wave, u_0 will be a series of Dirac impulses of magnitude g, alternatively positive and negative. Assuming that the noise w is uncorrelated with d, ensemble averaging of the signals $u_{n\#}$ after alternate compensation of the sign of the Dirac impulses directly provides the impulse response $g_n(k)$ of the transfer functions G_n. In other words, one has:

$$\begin{aligned} G_n &= \frac{1}{g}\left[g_n(0) + z^{-1} g_n(1) + \cdots + z^{-k} g_n(k)\right] \\ &= \frac{1}{g}\sum_k z^{-k} g_n(k) \end{aligned}$$

To illustrate the behavior of the cooperative-sensor system, Fig. 5 to Fig. 7 shows a set of experimental data acquired on a patient simulator—Seculife PS200 (Gossen Metrawatt, Nürnberg, Germany)—which simulates the ECG voltage sources $u_{ECG,n}$ of Fig. 3. Fig. 8 shows the response of G_n for an impulse of magnitude g (ensemble averaging of $u_{n\#}$).

The transfer function G_1 is slightly different, because the series of alternatively positive and negative Dirac impulses of magnitude g results in a square wave of $\pm g_1$ (see Fig. 9).

$$G_1 = \frac{2g_1}{g}\frac{z}{z-1}$$

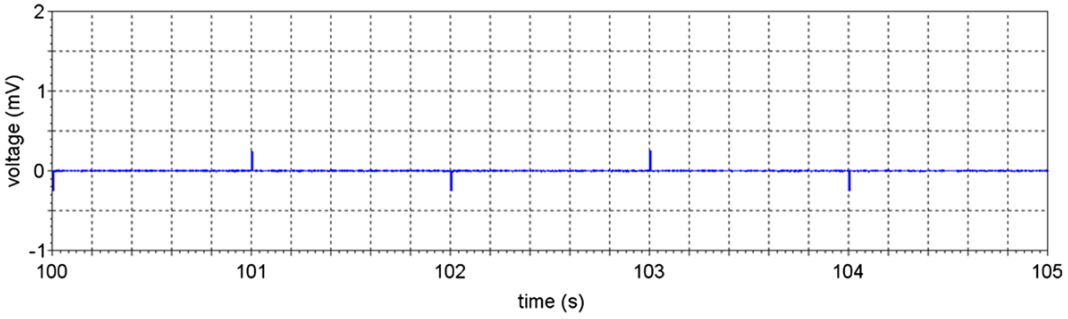

Figure 5: Signal u_0, i. e., series of alternate impulses of magnitude g.

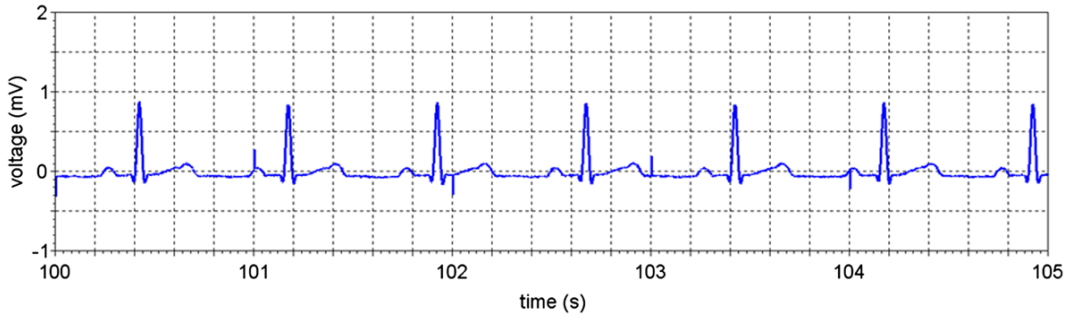

Figure 6: Signal u_n (*with* $n \in \{2, ..., N\}$), i. e., $u_{\mathrm{ECG},n}$ superimposed with series of alternate impulse of magnitude g.

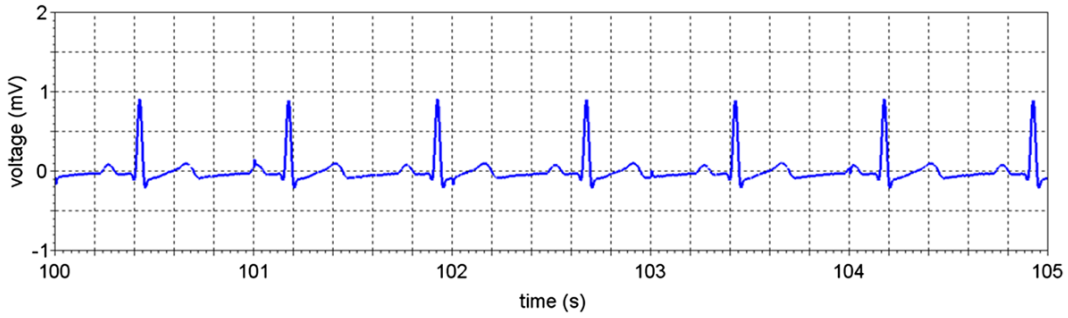

Figure 7: Signal $u_{n\#}$ (*with* $n \in \{2, ..., N\}$, gain in bandwidth reported to input of G_n), i. e., signal u_n filtered by G_n (with gain normalized to unity).

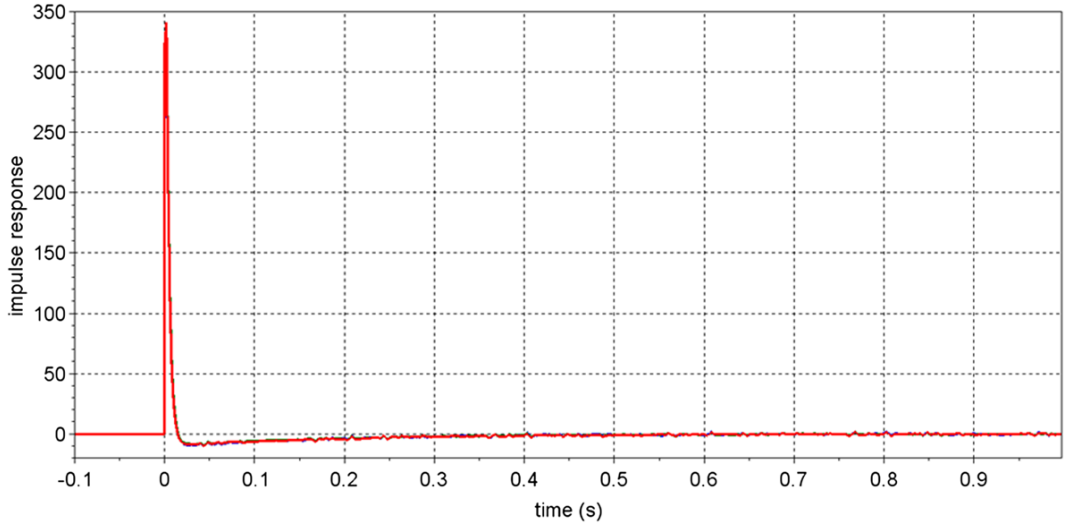

Figure 8: Ensemble averaging of $u_{n\#}$ (*with* $n \in \{2, ..., N\}$), i. e., response of G_n for impulse of magnitude g.

Taking into account that we also have $G_1 = 1/s\tau$, one obtains:

$$g_n = \frac{2g_1\tau}{T}$$

where T is the sample period. The ensemble averaging used to obtain the coefficient $g_n(k)$ are ideally implemented with a forgetting factor starting with the best guess, i. e., the coefficients corresponding to the electronic circuit implementing G_n. The update rate of $g_n(k)$ should be smaller and smaller as k increases, because for large k, the impulse response vanishes and is therefore more sensitive to noise. In order to simplify the algorithms, sev-

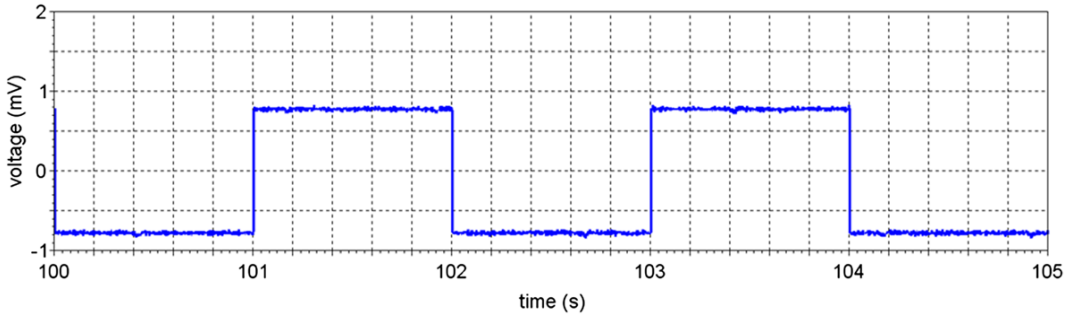

Figure 9: Signal $u_{1\#}$ representing a square-wave signal.

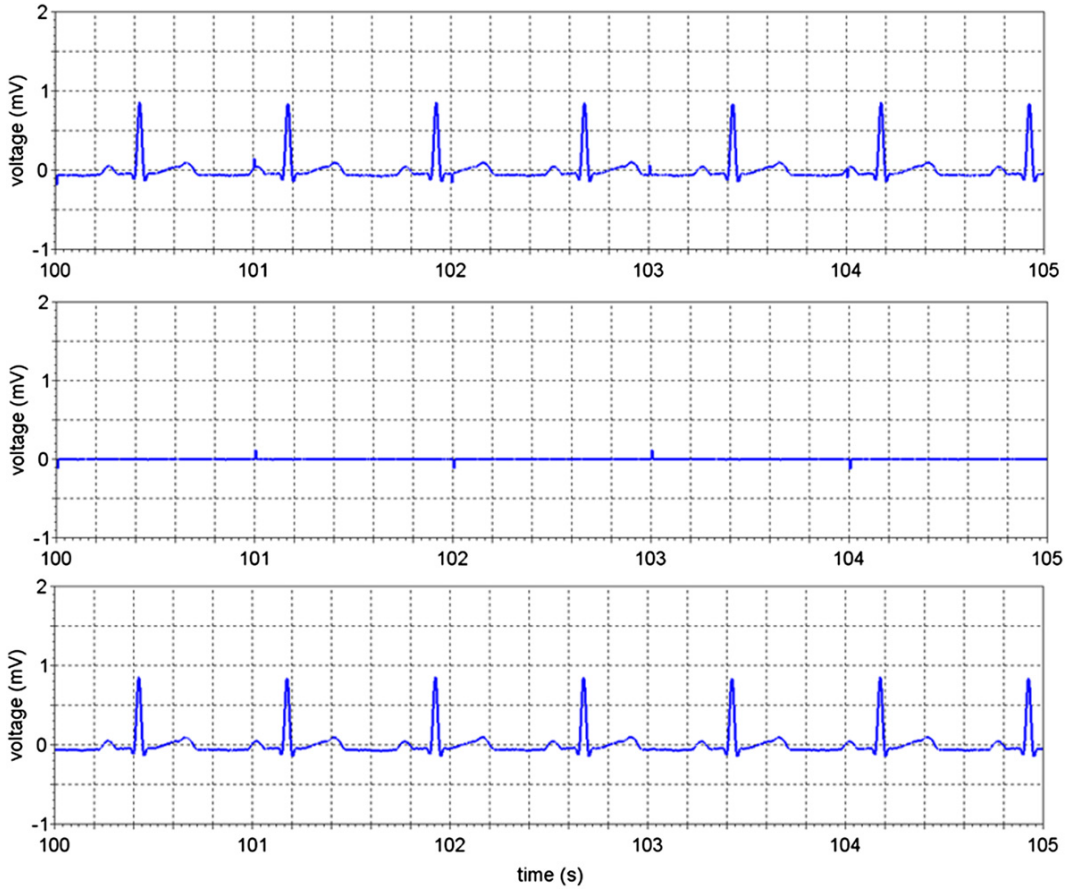

Figure 10: Higher plot: signal U_n (*with* $n \in \{2, ..., N\}$) corresponding to the signal measured by the n^{th} type V sensor. Middle plot: signal U_1 corresponding to the signal measured by the reference sensor. Lower plot: Signal $U_n - U_1$ corresponding to a measured ECG lead.

eral samples can be taken together for large k. The transfer function H_n is given by:

$$H_n = \frac{\tau\left(1-e^{-T/\tau_1}\right)\left(1-e^{-T/\tau_2}\right)}{2T}\frac{z^2-1}{\left(z-e^{-T/\tau_1}\right)\left(z-e^{-T/\tau_2}\right)G_n}$$
$$= \frac{g\tau_1\left(1-e^{-T/\tau_1}\right)\left(1-e^{-T/\tau_2}\right)}{2T} \times \frac{z^2-1}{\left(z-e^{-T/\tau_1}\right)\left(z-e^{-T/\tau_2}\right)\sum_k z^{-k}g_n(k)}$$

where τ_1 the time constant corresponding to the low corner frequency (0.05 Hz) and τ_2 the time constant corresponding to the high corner frequency (150 Hz).

Fig. 10 shows the signals measure by the n^{th} type V sensors (higher plot) and the reference sensor (middle plot), as well as an example of a computed ECG lead (lower plot). As expected, the excitation signal d is not visible in the final ECG lead since this lead results from the difference between two measured signals.

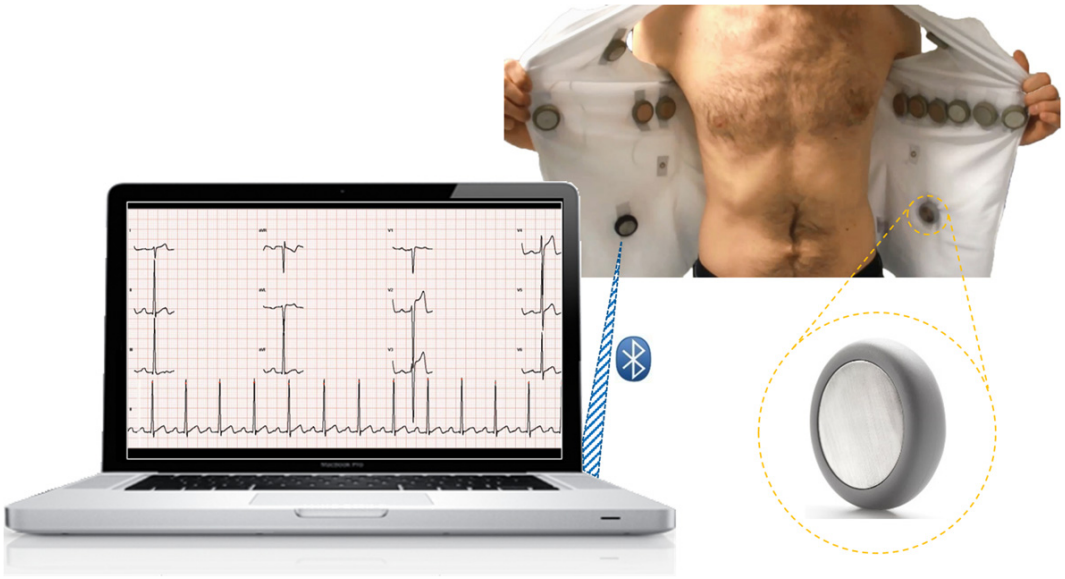

Figure 11: Realization of a 12-lead ECG Holter with cooperative sensors. The ECG signals are measured by the reference sensor (as u_1), and by the eight type V sensors (as u_2 to u_9). The measured data are gathered in the master sensor via the two-wire communication bus and transferred in real time via a Bluetooth communication to a smart device for processing, recording, and monitoring purpose.

In the current implementation of the system, the achieved precision of the gain of the cooperative sensors (P_G) is of about 0.1 % leading to a global CMRR of the system of 98 dB (with $\mathrm{CMRR_D} = 54$ dB).

3 Experimental results

This section shows the realization of a 12-lead ECG Holter with cooperative sensors. The cooperative-sensor system was compared to a gold-standard medical device during an exercise stress test.

3.1 System integration in a 12-lead ECG Holter

A wearable 12-lead ECG monitoring system (an ECG Holter) based on the cooperative-sensor circuit presented in Fig. 3 was integrated in a vest (see Fig. 11). It is made of one master, one reference, and eight type V sensors, and uses the common-mode rejection principle described in this paper. The ECG voltages are measured as u_1 in the reference sensor, and as u_2 to u_9 in the type V sensors. The sensors are attached to the vest using their two snap buttons. The ref. and com. wires are two unshielded wires integrated in the textile of the vest. Each sensor has a single skin-contact which is implemented as a stainless-steel dry electrode (diameter 28 mm). To comply with the Mason-Likar configuration for modified 12-lead ECG monitoring systems [16], the master sensor is placed onto the skin at the RL location, the reference sensor at the LL location, and the eight type V sensors are placed at the RA, LA, and the six precordial locations (V1 to V6). To comply with the IEC international standard for ECG measurement (IEC 60601-2-25), the sampling rate of the measured ECG is 500 Hz and its bandwidth is limited between 0.05 and 150 Hz. It has to be noted that an analog band-pass filter is applied on each measured ECG signals prior to their amplification and analog to digital conversion.

3.2 Comparison during exercise stress test

The goal of this test is to qualitatively assess the ECG performance of the dry-electrode cooperative-sensor system during exercise stress test performed on a stationary bicycle ergoselect200 (ergometer from Ergoline, Bitz, Germany). This exercise stress test was performed on four healthy male subjects with the setup shown in Fig. 12. A gold-standard 12-lead ECG system—the Cardiovit CS-200 (Schiller, Baar, Switzerland)—was used as a reference. The limb electrodes (LA, RA, LL, and RL) were placed at locations as close as possible to those of cooperative sensors.

Fig. 13 shows ECG signals (measured on leads I, II, and III) obtained from the medical device (black signals) and from the dry-electrode cooperative sensors (red signals) during the exercise stress test. As a first qualitative obser-

Figure 12: Test setup with both the cooperative-sensor system and the gold-standard medical device (Cardiovit CS-200) connected to the subject (left) and subject performing the exercise stress test (right).

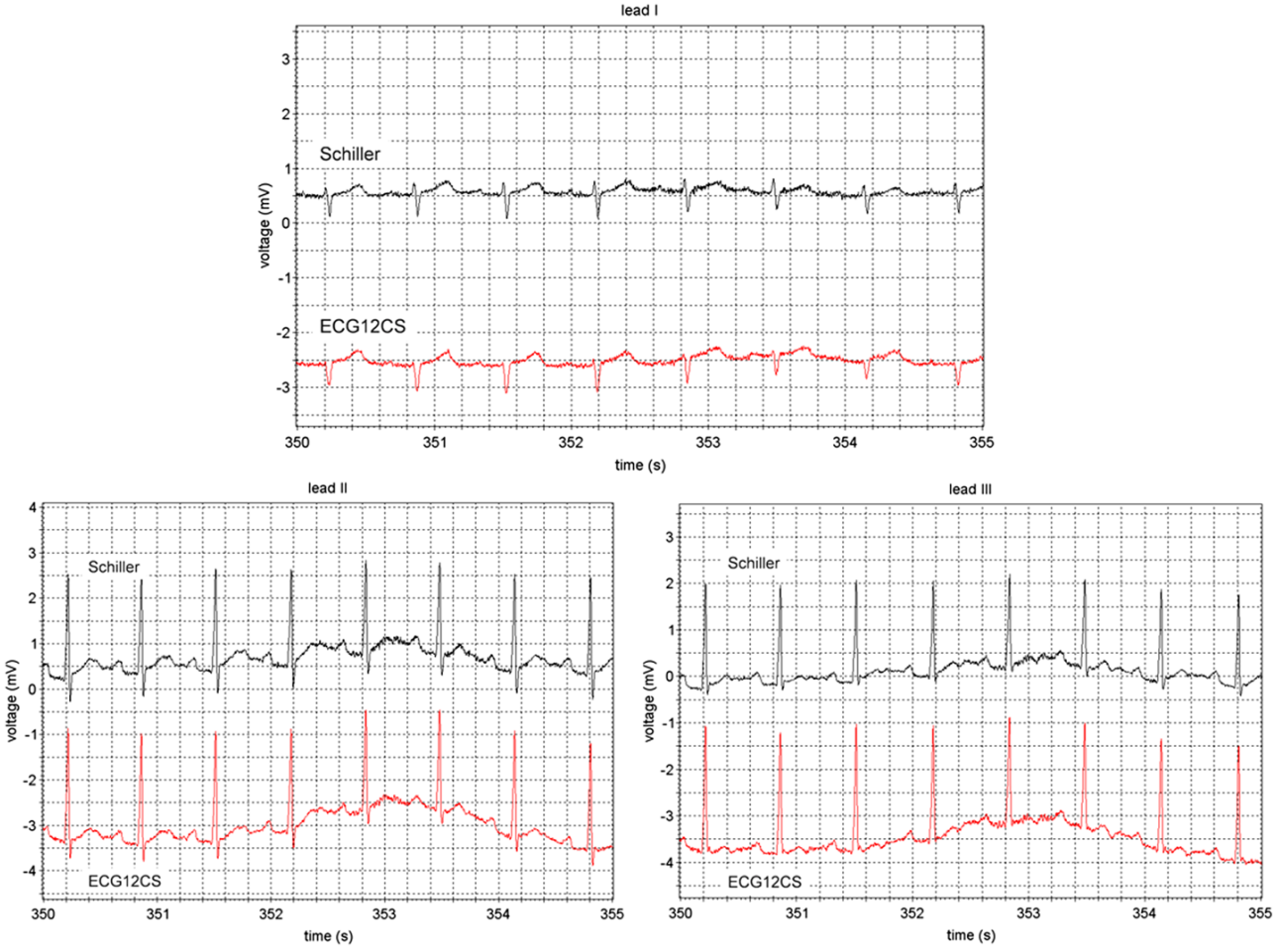

Figure 13: Comparison of typical ECG signals measured on leads I, II, and III with the Cardiovit CS-200 (black signals) and the dry-electrode cooperative-sensor system (red signals).

vation, these figures show that the two signals are very similar. When there is some noise on the signals, it appears on both of them simultaneously (which means that the electrical artifact is already present on the body).

4 Discussion and conclusion

This paper presents an enhanced common-mode rejection method based on a novel multilead ECG sensing architecture (so-called cooperative sensors). In the cooperative-sensor architecture, the transfer functions of each measuring sensor may differ due to the mismatch of the electrical component used in each sensor. Another parameter that may impart the transfer function over time is the voltage divider embodied by the skin impedance and the input impedance of the analog frontend used to sense the ECG voltages. To overcome this issue, this paper depicted a solution for the auto-identification and the rectification of the transfer functions of the cooperative-sensor system. This method allows a continuous-time rectification of the transfer function mismatch, and thus to improve the global CMRR of the cooperative sensor system.

It has to be noted that, even without the proposed auto-calibration method, the cooperative-sensor system can reach a CMRR of 78 dB (see section 2.2) with a reasonable matching between the sensors (i. e., with $P_G = 0.01$). This CMRR already complies with the international standard for ambulatory ECG (IEC 60601-2-47), which states that the minimal CMRR shall be at least 60 dB. However, this method is fully realized if a higher CMRR is required (e. g., for a clinical ECG monitoring device), or if we use lower precision components (e. g., in view of the integration of the system in an ASIC, where gain mismatches between chips can easily reach ±10 % at cut-off frequencies).

This paper demonstrates the feasibility of measuring a 12-lead ECG in a real-life scenario with the proposed common-mode rejection method. The cooperative-sensor system contains one master, one reference, and eight type V sensors connected via a two-wire bus. Even though the wires that link all sensors are not shielded, they do not interfere with each other and there is no mains disturbance visible in the measured signals (see Fig. 13). Moreover, measurements showed that the dry-electrode cooperative-sensor technology provides signals of quality at least equivalent to conventional 12-lead ECG medical devices. Although this paper focuses on the application of cooperative sensors for ECG measurement, the same architecture is fully applicable to the assessment of other biopotentials (e. g., EMG or EEG), or other physiological signals such as bioimpedance.

References

1. N. Bashi, M. Karunanithi, F. Fatehi, H. Ding and D. Walters, "Remote Monitoring of Patients With Heart Failure: An Overview of Systematic Reviews," J. Med. Internet. Res., vol. 19, no. 1, pp. 1–14, Jan. 2017.
2. G. Pare, M. Jaana and C. Sicotte, "Systematic Review of Home Telemonitoring for Chronic Diseases: The Evidence Base," J. Am. Med. Inform. Assoc., vol. 14, no. 3, pp. 269–277, May 2007.
3. B. G. Celler and R. S. Sparks, "Home Telemonitoring of Vital Signs - Technical Challenges and Future Directions," IEEE J. Biomed. Health Inform., vol. 19, no. 1, pp. 82–91, Jan. 2015.
4. J. Cruz, D. Brooks and A.Marques, "Home telemonitoring in COPD: A systematic review of methodologies and patients' adherence," Int. J. Med. Inf., vol. 83, no. 4, pp. 249–263, Apr. 2014.
5. Y.-L. Zheng et al., "Unobtrusive sensing and wearable devices for health informatics," IEEE Trans. Biomed. Eng., vol. 61, no. 5, pp. 1538–1554, May 2014.
6. A. C. M. van Rijn, A. Peper and C. A. Grimbergen, "High-quality recording of bioelectric events," Med. Biol. Eng. Comput., vol. 29, no. 4, pp. 433–440, Jul. 1991.
7. T. Degen, S. Torrent and H. Jäckel, "Low-Noise Two-Wired Buffer Electrodes for Bioelectric Amplifiers," IEEE Trans. Biomed. Eng., vol. 54, no. 7, pp. 1328–1332, Jul. 2007.
8. J. Xu, B. Busze, C. Van Hoof, K. A. A. Makinwa and R. F. Yazicioglu, "A 15-Channel Digital Active Electrode System for Multi-Parameter Biopotential Measurement," IEEE J. Solid-State Circuits, vol. 50, no. 9, pp. 2090–2100, Sep. 2015.
9. G. Yang, J. Chen, Y. Cao, H. Tenhunen and L.-R. Zheng, "A novel wearable ECG monitoring system based on active-cable and intelligent electrodes," in HealthCom 2008 — 10th International Conference on e-Health Networking, Applications and Services, pp. 156–159, Jul. 2008.
10. M. Rapin et al., "Two-wire bus combining full duplex body-sensor network and multilead biopotential measurements," IEEE Trans. Biomed. Eng., vol. 65, no. 1, pp. 113–122, Jan. 2018.
11. M. Rapin, D. Ferrario, E. Haenni, J. Wacker, A. Falhi, C. Meier, J.-A. Porchet and O. Chételat, "Electromagnetic disturbances rejection with single skin contact in the context of ECG measurements with cooperative sensors," in 2017 39th Annual International Conference of the IEEE Engineering in Medicine and Biology Society (EMBC), pp. 4427–4430, Jul. 2017.
12. T. Degen and H. Jäckel, "Continuous Monitoring of Electrode–Skin Impedance Mismatch During Bioelectric Recordings," IEEE Trans. Biomed. Eng., vol. 55, no. 6, pp. 1711–1715, Jun. 2008.
13. P. Zipp and H. Ahrens, "A model of bioelectrode motion artefact and reduction of artefact by amplifier input stage design," Journal of Biomedical Engineering, vol. 1, no. 4, pp. 273–276, Oct. 1979.

14. Y. M. Chi, T. P. Jung and G. Cauwenberghs, "Dry-Contact and Noncontact Biopotential Electrodes: Methodological Review," IEEE Rev. Biomed. Eng., vol. 3, pp. 106–119, Oct. 2010.
15. T. Degen and H. Jäckel, "A Pseudodifferential Amplifier for Bioelectric Events With DC-Offset Compensation Using Two-Wired Amplifying Electrodes," IEEE Trans. Biomed. Eng., vol. 53, no. 2, pp. 300–310, Feb. 2006.
16. J. S. Steinberg, N. Varma, I. Cygankiewicz, P. Aziz, P. Balsam, A. Baranchuk, D. J. Cantillon, P. Dilaveris, S. J. Dubner, N. El-Sherif, J. Krol, M. Kurpesa, M. T. La Rovere, S. S. Lobodzinski, E. T. Locati, S. Mittal, B. Olshansky, E. Piotrowicz, L. Saxon, P. H. Stone, L. Tereshchenko, G. Turitto, N. J. Wimmer, R. L. Verrier, W. Zareba and R. Piotrowicz, "2017 ISHNE-HRS expert consensus statement on ambulatory ECG and external cardiac monitoring/telemetry," Heart Rhythm., vol. 14, no. 7, pp. e55–e96, Jul. 2017.

Bionotes

Michaël Rapin
Laboratory for Orthopedic Biomechanics, Swiss Federal Institute of Technology in Zurich (ETHZ), Zürich 8092, Switzerland
Centre Suisse d'Electronique et de Microtechnique (CSEM), Neuchatel 2002, Switzerland
mir@csem.ch

Michaël Rapin got a Master in electrical engineering from the Swiss Institute of Technology (EPFL), Lausanne, Switzerland in 2012. Since then, he joined CSEM where he developed electronics related to physiological parameter measurement such ad bioimpedance, ECG, and sounds of heart and lungs. He obtained in 2014 a PhD grant from ESA to develop the concept of cooperative sensors. He is currently finishing his PhD at the Swiss Federal Institute of Technology (ETHZ), Zürich, Switzerland.

Yves-Julien Regamey
Centre Suisse d'Electronique et de Microtechnique SA, Rue Jaquet-Droz 1, CH-2002 Neuchatel, Switzerland

Yves-Julien Regamey received the PhD degree in Mechatronics from the Swiss Institute of Technology, Lausanne, Switzerland in 2005. He joined CSEM in 2013 where he works as a senior control engineer in fields involving, mathematical modelization, optimization, and/or software development for control applications, mechanical system, and bioengineering.

Olivier Chételat
Centre Suisse d'Electronique et de Microtechnique SA, Rue Jaquet-Droz 1, CH-2002 Neuchatel, Switzerland
och@csem.ch

Dr. Olivier Chételat received the PhD degree in robotics from the Swiss Institute of Technology, Lausanne, Switzerland in 1997. He spent one year as post-doctoral fellow in the USA (1998) and two years as assistant professor in Korea (2000/2001). He joined CSEM in 2001 where he has been involved in the management of several projects, in particular ESA projects related to vital parameter monitoring. Besides, he played an active role as technical expert in several research programs, including European projects and commercial projects focused on ECG, impedance, SpO2, and core body temperature sensors. Since 2009, he has been section head of Electronics and Research manager of the MEDTECH activity.